

Review

Research Progress on New Types of H_2TiO_3 Lithium-Ion Sieves: A Review

Ying Li ^{1,2,*}, Zhen Yang ^{1,2} and Peihua Ma ¹¹ School of Metallurgy, Northeastern University, Shenyang 110819, China; 1910535@stu.neu.edu.cn (Z.Y.)² Liaoning Key Laboratory for Metallurgical Sensor Materials and Technology, Northeastern University, Shenyang 110819, China

* Correspondence: liying@mail.neu.edu.cn

Abstract: The advantages of new types of H_2TiO_3 lithium-ion sieves, including excellent adsorption performance, high-efficiency Li^+ -ion selectivity, reliable regeneration, environmental friendliness, and easy preparation, have attracted considerable attention. Currently, the prices of lithium carbonate and other related products are rapidly increasing, so the use of H_2TiO_3 lithium-ion sieves to extract lithium resources in salt lake brine has become a crucial strategy. H_2TiO_3 lithium-ion sieve is a layered double hydroxide with a $3R_1$ sequence to arrange oxygen layers. Its adsorption mechanism involves the breaking of surface O-H bonds and the formation of O-Li bonds. This study provides a theoretical basis for developing high-efficiency lithium-ion sieves. This article also summarizes the influencing factors for the synthesis process of H_2TiO_3 , which can seriously influence the adsorption performance, and offers experimental verification for the preparation of H_2TiO_3 lithium-ion sieves. H_2TiO_3 lithium-ion sieves prepared from anatase using a reasonable method show the largest adsorption capacity. In addition, effective ways to recycle H_2TiO_3 are outlined, which provide a guarantee for its industrial application. Finally, this paper summarizes the full text and points out future research directions for H_2TiO_3 lithium-ion sieves.

Keywords: Li; H_2TiO_3 lithium-ion sieve; crystal structure; adsorption mechanism; influencing factors; recycling



Citation: Li, Y.; Yang, Z.; Ma, P. Research Progress on New Types of H_2TiO_3 Lithium-Ion Sieves: A Review. *Metals* **2023**, *13*, 977. <https://doi.org/10.3390/met13050977>

Academic Editor: Felix A. Lopez

Received: 7 April 2023

Revised: 10 May 2023

Accepted: 16 May 2023

Published: 18 May 2023



Copyright: © 2023 by the authors. Licensee MDPI, Basel, Switzerland. This article is an open access article distributed under the terms and conditions of the Creative Commons Attribution (CC BY) license (<https://creativecommons.org/licenses/by/4.0/>).

1. Introduction

Lithium has become the most important strategic resource, and it shows outstanding performance in the field of new energy. Lithium-ion batteries occupy a large proportion of new energy fields, forming a three-legged situation based on LiFePO_4 [1,2], LiMn_2O_4 [3,4], and $\text{LiNi}_x\text{Co}_y\text{Mn}_z\text{O}_2$ [5–12], resulting in rising prices. Lithium can also be added to alloys to form ultralight alloys, such as aluminium–lithium alloys [13] and magnesium–lithium alloys [14]. It can also be used to prepare greases [15], form optical components [16], produce low-expansion-coefficient foam ceramics [17,18], etc.

Lithium has many existing forms, so researchers need to conduct in-depth research into the extraction of lithium resources from different environments. These include extraction from lithium mines [19,20], salt lake brine [21–23], and shale gas-produced water [24–26]. Compared with liquid lithium resources, the content of solid lithium resources is lower, so extraction from liquid lithium deposits has more significant development potential. There are many ways to extract lithium resources from liquid lithium ore, such as extraction [27–29], membrane separation [30,31], precipitation [32], electrochemistry [33–35], use of aluminium-based adsorbents [36–39], and manganese-based [40–43] and titanium-based [44,45] lithium-ion sieves.

There have been relatively more studies on manganese-based lithium-ion sieves, while few investigations have been carried out for titanium-based sieves. $\lambda\text{-MnO}_2$, $\text{MnO}_2 \cdot 0.3\text{H}_2\text{O}$, and $\text{MnO}_2 \cdot 0.5\text{H}_2\text{O}$ have theoretical adsorption capacities of 39.6, 59.0, and 72.9 mg/g, respectively. There is a severe disproportionation reaction in manganese-based lithium-ion

sieves, and the dissolution of Mn^{2+} under acidic conditions has become the main obstacle that hinders its industrial application. The theoretical adsorption capacity of manganese-based lithium-ion sieves compared with Ti-based lithium-ion sieves is relatively low. Ti^{4+} in $H_4Ti_5O_{12}$ has chemical stability, but the theoretical adsorption capacity is 63.77 mg/g, which is lower than that of H_2TiO_3 . The H_2TiO_3 lithium-ion sieve has a theoretical adsorption capacity of 142.9 mg/g. Ti^{4+} has high stability, avoiding disproportionation reactions and the Jahn–Teller effect, which results in low titanium dissolution loss and excellent recycling performance. Therefore, developing a new type of titanium-based lithium-ion sieve is significant for the extraction of lithium resources.

In this paper, Section 2 focuses on the crystal structure and adsorption mechanism of H_2TiO_3 lithium-ion sieves, Section 3 concerns the factors influencing the adsorption performance during the synthesis process, Section 4 reviews the methods for efficient recycling, and Section 5 draws conclusions and outlooks. The representative research work in recent years is reviewed, and a future direction for development is proposed.

This paper focuses on the adsorption mechanism of H_2TiO_3 lithium-ion sieves and the factors affecting their adsorption performance while at the same time focusing on their efficient recycling. Clear ideas are provided for the preparation and industrial application of high-performance and recyclable H_2TiO_3 .

2. Crystal Structure and Adsorption Mechanism for H_2TiO_3

2.1. Crystal Structure of H_2TiO_3

The H_2TiO_3 lithium-ion sieves are obtained by eluting Li_2TiO_3 with an acid solution, so it is necessary to analyse the structure of Li_2TiO_3 first. As shown in Figure 1a, the crystal structure of Li_2TiO_3 is a layered monoclinic structure with a space group of $C2/c$, O atoms that are arranged in cubic close-packed lattices, and Ti atoms that are located in the octahedral gap of O atoms, forming $[TiO_6]$ octahedra. Li atoms are fixed in two positions, and Li atoms at different sites have different chemical activities. In total, 25% of the Li atoms are located between two adjacent $[TiO_6]$ octahedra to form $(LiTi_2)$ layers, 75% of the Li atoms form pure Li layers, and $(LiTi_2)$ layers are alternately arranged with pure Li layers. Therefore, Li_2TiO_3 can be described as $Li[Li_{1/3}Ti_{2/3}]O_2$, indicating that it has a layered structure [46].

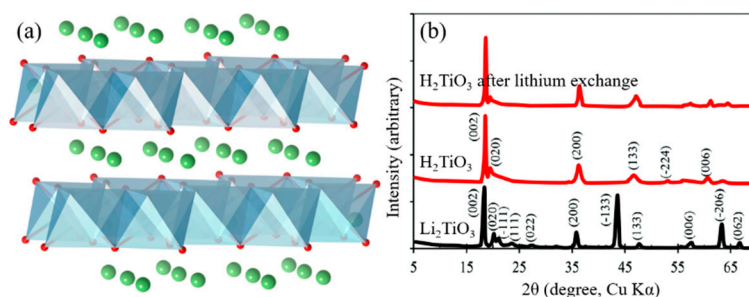
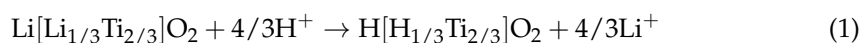


Figure 1. Crystal structure and XRD patterns: (a) crystal structure of Li_2TiO_3 ; (b) XRD patterns for Li_2TiO_3 , H_2TiO_3 , and H_2TiO_3 after lithium exchange [47].

Li_2TiO_3 was placed in a 0.5 M HCl solution at 25 °C after 24 h. After stirring, the suspension was filtered, washed with deionized water until neutral, and then dried at 105 °C to obtain H_2TiO_3 . The process can be expressed as follows:



From Equation (1), it can be seen that the H^+ in solution completely exchanges with the Li atoms in the pure Li layer and the Li atoms in the $(LiTi_2)$ layer to form the H_2TiO_3 lithium-ion sieve.

Li et al. [48] conducted FTIR analysis of Li_2TiO_3 and H_2TiO_3 to research the structure variation, as shown in Figure 2a, and found that the peaks at 1508 cm^{-1} and 1439 cm^{-1}

are due to the characteristic vibrations of Li-O bonds. After acid pickling, these two characteristic peaks disappear, indicating rupture of the Li-O bond. The band at 3477 cm^{-1} corresponds to the stretching vibration of weakly hydrogen-bonded OH related to $\text{Li}^+\text{-H}^+$ ion exchange. Wang et al. [49] found the same phenomenon in a study of lithium-enriched $\beta\text{-Li}_2\text{TiO}_3$, as shown in Figure 2b.

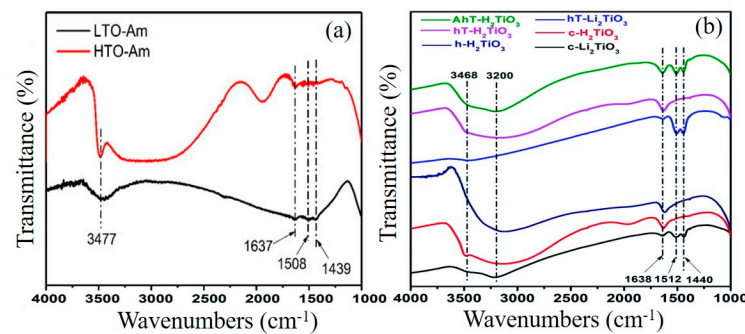


Figure 2. FTIR spectra: (a) FTIR spectra for LTO-Am and HTO-Am; (b) FTIR spectra for $\beta\text{-Li}_2\text{TiO}_3$ and H_2TiO_3 [48,49].

H atoms in the acid solution replace all the Li atoms in Li_2TiO_3 , thus producing two types of H atoms with different chemical reactivities. He et al. [50] and Ji et al. [51] reported that the H atoms located in the (HTi₂) layer cannot be re-exchanged for Li^+ , thereby showing a much lower lithium adsorption capacity than the theoretical adsorption capacity of the H_2TiO_3 lithium adsorbent.

Chitrakar et al. [52] found that the XRD pattern for H_2TiO_3 is similar to that of the Li_2TiO_3 precursor. The lattice parameters were found to be in good agreement with the reported values for H_2TiO_3 . H_2TiO_3 adopts a layered monoclinic structure (space group $C2/c$). However, Yu et al. [47] did not agree with Chitrakar's analysis. As shown in Figure 1b, the XRD patterns for H_2TiO_3 differ substantially from those of the Li_2TiO_3 precursor. Among these peaks, the $(\bar{1}33)$ and $(\bar{2}06)$ peaks are essential. These two peaks will always preferentially develop in the XRD patterns obtained for Li_2TiO_3 powders via wet chemistry processing methods. The (002) and $(\bar{1}31)$ peaks also show the same trend. Zhang et al. [53,54] obtained the same results through first-principles calculations and experiments. Further analysis found that H_2TiO_3 is a layered double hydroxide with a $3R_1$ sequence for the arrangement of oxygen layers, which can be described as a stacking of charge-neutral metal oxyhydroxide slabs $[(\text{OH})_2\text{OTi}_2\text{O}(\text{OH})_2]$. More experimental verification is required to confirm the well-refined structure.

By thoroughly analysing the crystal structure of the H_2TiO_3 lithium adsorbent, we recognize the adsorbent, and we can drive targeted research to enhance its adsorption performance. It is also feasible to design more common adsorbents based on this adsorbent structure, which are not limited to Li^+ adsorbents, thus greatly expanding the research field.

2.2. Adsorption Mechanism for H_2TiO_3

We can express the adsorption process for H_2TiO_3 as follows:

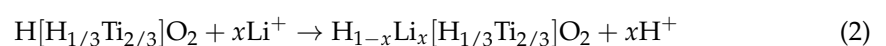


Figure 3 shows the schematic adsorption mechanism for the H_2TiO_3 lithium-ion sieve. Liu et al. [55] reviewed the adsorption mechanism for titanium-based lithium-ion sieves and considered that H_2TiO_3 conducts Li^+ ions that are adsorbed through the ion exchange mechanism. He et al. [50] reported that the ion exchange involves a typical electrostatic attraction without breaking any chemical bonds, as shown in Figure 3a. However, Marthi et al. [56] proposed a contrary lithium adsorption mechanism in which lithium adsorption involves the breaking of surface O-H bonds and the formation of O-Li bonds, as shown in Figure 3b.

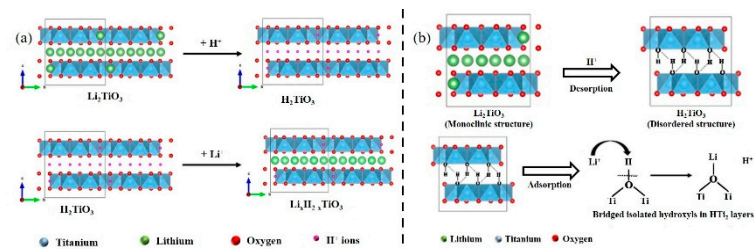


Figure 3. Lithium adsorption mechanism: (a) traditional lithium adsorption mechanism; (b) lithium adsorption mechanism proposed by Marthi [56].

Figure 4a,b show the XPS spectra for O 1s. Wang et al. [57] found that Mo doping leads to an increase in the O^{2-} content from 53.26% to 61.58%, and the adsorption capacity is increased to 78 mg/g, implying that the O^{2-} content is related to the adsorption performance. Wang et al. [49] also used the hydrothermal method to synthesize lithium-rich monoclinic lithium-enriched β - Li_2TiO_3 . As shown by the XPS spectra in Figure 4c,d, the higher the O^{2-} content, the more Li^+ adsorption sites there are, suggesting a higher adsorption capacity. He believes that the higher the O^{2-} content of lithium-ion sieves, the more lithium adsorption sites there are and the better the adsorption performance. This highlights one principle for designing high adsorption capacity lithium-ion sieves.

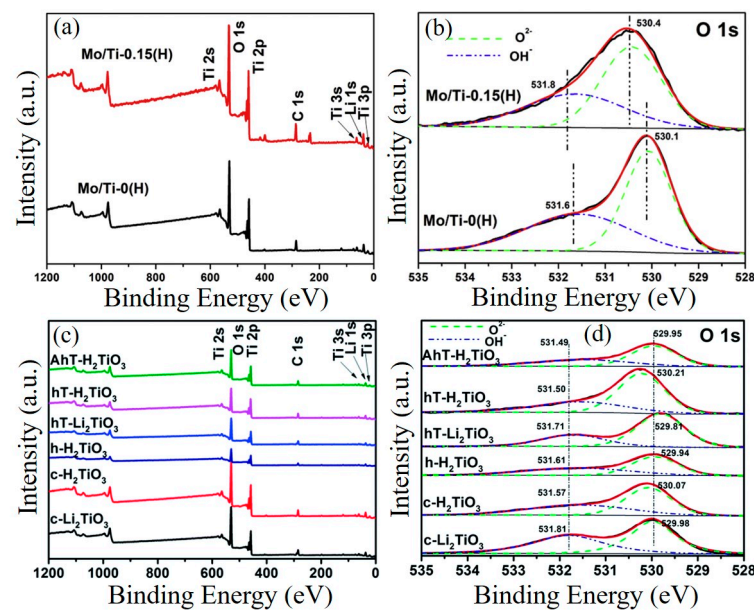


Figure 4. XPS spectra for H_2TiO_3 doped by Mo and β - Li_2TiO_3 , H_2TiO_3 : (a) XPS spectra for the full region of H_2TiO_3 doped by Mo; (b) O 1s fitted XPS spectra for H_2TiO_3 doped by Mo; (c) XPS spectra for the full region of β - Li_2TiO_3 , H_2TiO_3 ; (d) O 1s fitted XPS spectra for β - Li_2TiO_3 , H_2TiO_3 [49,57].

Summary of the kinetics and isotherm adsorption process for H_2TiO_3 . An agreement has been reached for the adsorption kinetics, which can be described with the pseudo-second-order model and belong to the chemical adsorption process. The isotherm adsorption process is more in line with the Langmuir isotherm adsorption model. Marthi et al. [58] designed $H_2TiO_3@DE$ (diatomaceous earth) and found that the surface energies of the active sites are heterogeneously distributed. The Freundlich model shows a better fit than the Langmuir model.

3. Influence of the H_2TiO_3 Synthesis Process on Adsorption Performance

The synthesis procedure of the H_2TiO_3 adsorbent contains two parts: the synthesis of Li_2TiO_3 and the acid-eluting process. Both of these steps significantly influence the

adsorption performance. Most Li_2TiO_3 is synthesized using the solid-phase method, and the sol-gel and hydrothermal methods have been used for synthesis in only a few cases. It is essential to investigate various aspects and provide theoretical support for synthesizing high-performance H_2TiO_3 .

3.1. The Influence of Ti Sources

TiO_2 is the raw material for synthesizing the H_2TiO_3 adsorbent, and it has three crystal phases: amorphous, anatase, and rutile. Diverse crystal phases have varying influence on the crystal structure. Zhang et al. [59] calcined metatitanic acid at the designed temperatures (25~1050 °C) to prepare TiO_2 with different crystal phases. The XRD patterns are shown in Figure 5a. Prior to the reaction, the mixture of TiO_2 and $\text{LiOH}\cdot\text{H}_2\text{O}$ in a molar ratio of 1/2 was wet ball milled for 5 h with anhydrous alcohol as a dispersant. After drying, the mixture was calcined at 750 °C for 5 h in a muffle furnace under an air atmosphere. Subsequently, the H_2TiO_3 -lithium adsorbent was obtained after hydrochloric acid treatment (0.25 M, 70 °C), filtration, washing, and drying. The XRD patterns are shown in Figure 5b. Figure 5c shows the pull-out rates for lithium from Li_2TiO_3 and the saturated adsorption capacity of the H_2TiO_3 -lithium adsorbent. Under the same pickling and adsorption conditions, the Li^+ drawn-out ratios are initially increased followed by a decrease with a maximum value of 98.69%, and the saturated adsorption capacity exhibits the same behaviour with a maximum value of 39.2 mg/g. As shown in Figure 5d, after comparison, the $[\text{TiO}_6]$ octahedron of Li_2TiO_3 is more similar to that of anatase than rutile, and only a small distortion associated with the transformation anatase $[\text{TiO}_6]$ - Li_2TiO_3 $[\text{TiO}_6]$ is needed. Because of the similarity between the $[\text{TiO}_6]$ of anatase and Li_2TiO_3 , a smaller energy barrier is required to form Li_2TiO_3 from anatase than from rutile. As a result, the Li_2TiO_3 structure prepared from anatase is more suitable for Li^+ extraction than that from rutile.

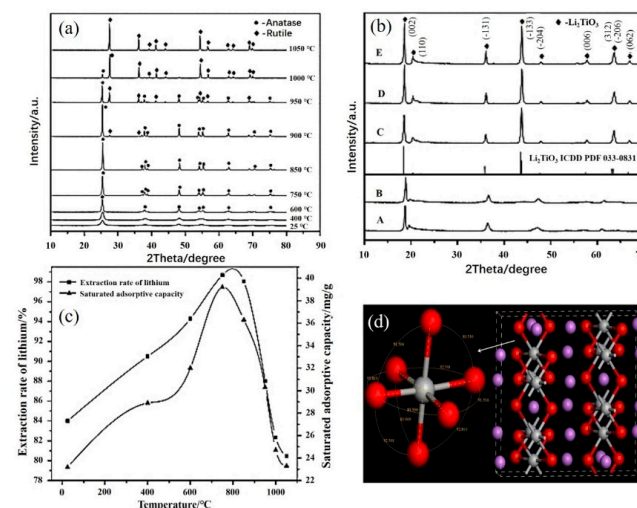


Figure 5. (a) XRD patterns for metatitanic acid at different temperatures; (b) XRD patterns for Li_2TiO_3 under various conditions; (c) extraction rates for Li^+ from Li_2TiO_3 and saturated adsorption capacity of the H_2TiO_3 -lithium adsorbent; (d) the cell structure and bond angles in the $[\text{TiO}_6]$ octahedron of Li_2TiO_3 [59].

Li et al. [60] found a correlation between the hydrophilicity and adsorption performance of the H_2TiO_3 adsorbent. Tetrabutyl titanate was slowly added dropwise into a mixed solution with stirring, and a white flocculent precipitate was produced. Then, the mixture was stirred at 40 °C for drying to obtain a white powder. The white powder was calcinated at 100 °C, 400 °C, and 1200 °C to obtain amorphous, anatase, and rutile TiO_2 . Li_2CO_3 and as-prepared TiO_2 with different crystal phases were mixed with a molar ratio of $\text{Li}:\text{Ti} = 2:1$ for 3 h. The mixture was placed into an alumina ark and roasted at 850 °C

for 5 h. A certain amount of Li_2TiO_3 was placed into a 0.2 M HCl solution at 60 °C for 10 h. After stirring, the suspension was filtered, washed with water until neutral, and then dried at 50 °C to obtain H_2TiO_3 . The adsorption capacities of H_2TiO_3 prepared by using the different crystal phases of TiO_2 were determined to be 17.11, 31.76, and 9.44 mg/g, respectively. Among these, the lithium-adsorbent designed using anatase shows the best adsorption performance. H_2TiO_3 synthesized using anatase shows the smallest contact angle, indicating excellent hydrophilicity of the substrate. Li^+ can be easily transported and exchanged with H^+ , thus achieving effective contact between H_2TiO_3 and Li^+ , as shown in Figure 6.

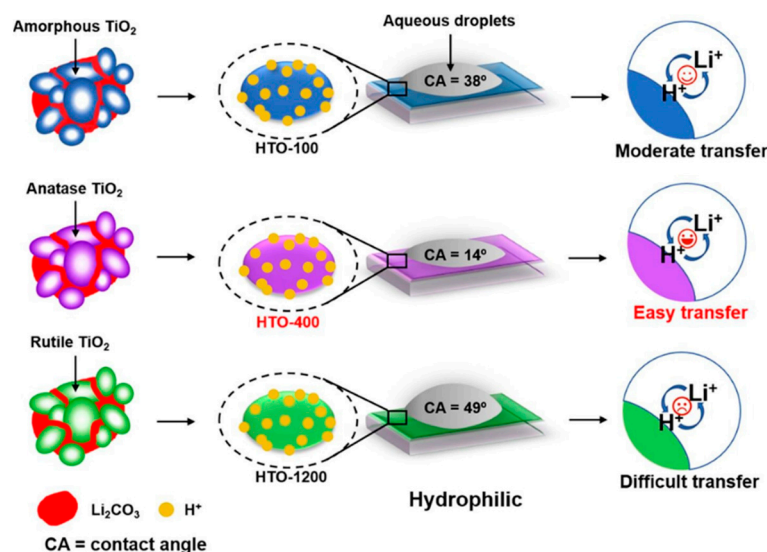


Figure 6. Schematic illustrations of the wettability of H_2TiO_3 for Li adsorption [60].

As shown above, the H_2TiO_3 adsorbent prepared by anatase TiO_2 has a higher adsorption capacity than other crystal phases, but Li et al. [48] synthesized H_2TiO_3 with better adsorption capacity through the use of amorphous TiO_2 . He obtained amorphous TiO_2 by hydrolysis of titanium (IV) isopropoxide and then mixed it with Li_2CO_3 to synthesize Li_2TiO_3 in a solid-phase reaction. An adsorption capacity of 30.03 mg/g was obtained through $\text{K}_2\text{S}_2\text{O}_8$ elution at 60 °C. This proved that amorphous TiO_2 also has the potential to prepare high adsorption capacity lithium adsorbents. It opens up a new window to synthesizing high-performance lithium-ion sieves.

All of us are pursuing high-performance H_2TiO_3 , but cost reduction is the goal pursued by enterprises. Tang et al. [61] purified low-grade titanium slag to obtain a Ti-rich material in which the TiO_2 content reached 88.35%. The H_2TiO_3 prepared from this Ti-rich material showed an adsorption capacity of 27.8 mg/g, which significantly reduces the cost of raw materials.

Marthi et al. [58] ground coarse titania slag into fine slag, sieved it to a size of 20 μm , and loaded it onto DE (diatomaceous earth). The lithium-ion sieve prepared with this material showed a maximum adsorption capacity of 27.4 mg/g. By using titania slag, one can prepare a lithium-ion sieve with high adsorption capacity that is easy to recycle when loaded onto DE. It is a lithium-ion sieve with an application value.

Table 1 lists the adsorption capacity of lithium adsorbents synthesized via different Ti sources. Different Ti sources can be used to successfully prepare lithium adsorbents with large adsorption capacities. Among them, lithium-ion sieves prepared from anatase show the largest adsorption capacity, and raw materials such as titanium slag are sufficient and have significant application prospects. Lithium-ion sieves synthesized from different Ti resources enrich the synthesis path for Ti-based lithium-ion sieves.

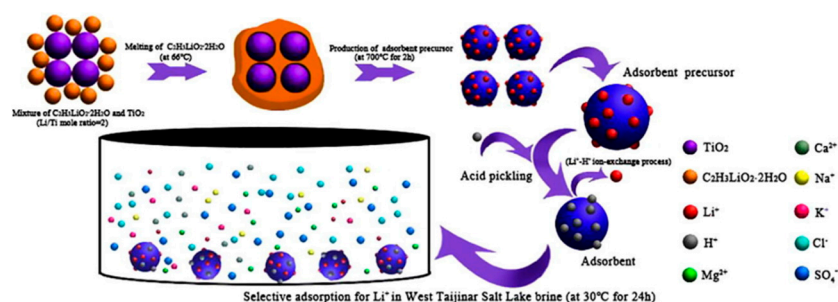
Table 1. Adsorption capacity of lithium adsorbents synthesized via different Ti sources.

Ti Sources	Sample	Li ⁺ Concentration (mg/L)	Adsorption Capacity (mg/g)	Ref.
Amorphous TiO ₂	LiCl solution	315.02	30.03	[48]
Coarse titania slag	Li ⁺ solution	50	27.4	[58]
Anatase TiO ₂	LiOH solution	2000	39.2	[59]
Tetrabutyl titanate	LiCl/LiOH solution	200	31.76	[60]
Titanium slag	LiOH solution	2000	27.8	[61]

3.2. The Influence of Synthesis Methods

Most H₂TiO₃ is synthesized using solid-phase methods [62], and sol-gel [63] and hydrothermal [49] methods have been used for synthesis in a few cases. Yu et al. [64] summarized three synthesis methods and found that the grain size of Li₂TiO₃ prepared using the solid-phase method is larger, and that the extraction of Li⁺ ions in Li₂TiO₃ prepared using the sol-gel method is more difficult. The saturated adsorption capacity of the H₂TiO₃ lithium-ion sieve prepared using the two methods is relatively low. In contrast, Li₂TiO₃ prepared using the hydrothermal method has a smaller grain size, stable structure, and high extraction rate for Li⁺ ions. However, there is a massive loss in the adsorption process with a small particle size, and recycling is challenging.

Although the hydrothermal method has many advantages, the solid-phase method is most suitable for large-scale industrial production, so it is essential to improve it appropriately. Gu et al. [65] replaced Li₂CO₃ with CH₃COOLi·2H₂O as the lithium source to mix with TiO₂, as shown in Figure 7. Melting CH₃COOLi·2H₂O (at 66 °C) during the early calcination stage can lead to the formation of a liquid–solid phase and remarkably improve the mixing of CH₃COOLi·2H₂O and TiO₂. In addition, the huge heat and gases released during the dehydration of CH₃COOLi·2H₂O and TiO₂ accelerate the nucleation process and effectively inhibit agglomeration, leading to a small particle size for Li₂TiO₃, and the ion exchange resistance is greatly reduced. H₂TiO₃ was obtained by eluting with acid solution at 70 °C for 8 h, with its adsorption capacity reaching a value of 24.97 mg/g in West Taijinar Salt Lake brine. The introduction of a low-temperature molten salt in the solid-phase method effectively improves the adsorption performance and can be used to prepare high-performance lithium-ion sieves.

**Figure 7.** H₂TiO₃ lithium-ion sieve synthesized via an improved solid-state method and adsorption process [65].

CH₃COOLi·2H₂O was successfully applied to synthesize H₂TiO₃ adsorbent by using the improved solid-phase method. Nevertheless, low-temperature molten salts are relatively few in number and expensive, which hinders the development of synthesis methods. As a common molten salt, LiCl can provide a melting environment for the solid-phase method, which dramatically reduces the restriction on lithium resources. Zhang et al. [66] mixed Li₂CO₃ with anatase TiO₂, added a certain amount of LiCl, placed the mixture into a corundum crucible, calcined at 650–950 °C for 10 h, and after washing with deionized water to remove LiCl salt, obtained Li₂TiO₃. H₂TiO₃ lithium-ion sieves were obtained through

HCl acid solution leaching of Li_2TiO_3 precursors. The preparation process for this lithium adsorbent results in fine grains and a large specific surface area due to the use of the molten salt. The adsorbent has an adsorption capacity of 28 mg/g in LiOH solution with pH = 12.

The adsorption performance of the H_2TiO_3 adsorbent depends on the material properties and specific surface area. Appropriate synthesis methods can be used to significantly enhance the adsorption capacity. Xu et al. [67] designed three-dimensional porous H_2TiO_3 lithium-ion sieves through the template method, as shown in Figure 8. The porous lithium-ion sieve has a specific surface area of $94.14 \text{ m}^2/\text{g}$. The adsorption capacity in the strong alkaline Bayer liquor is 70 mg/g, which is much higher than that of the bare lithium-ion sieve, indicating that the specific surface area dramatically influences the adsorption performance of the lithium-ion sieve. This provides an effective way to develop high adsorption capacity lithium-ion sieves and has great potential for industrial applications.

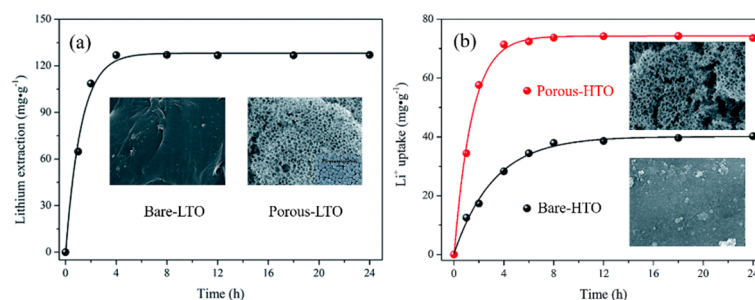


Figure 8. Lithium extraction and adsorption capacity: (a) lithium extraction rate from porous Li_2TiO_3 ; (b) Li^+ uptake for both bare H_2TiO_3 and porous H_2TiO_3 in the simulated Bayer liquor [67].

Table 2 lists the influence of the different synthesis methods on the adsorption capacity. Lithium-ion sieves prepared using different methods have different advantages and disadvantages. Among them, the solid-phase method is easy to apply and is suitable for large-scale industrial production, but the grain size of the lithium-ion sieve prepared using this method is relatively large, which is not conducive to adsorption. The sol-gel method can be used to produce smaller grain sizes, but the extraction of Li^+ ions is difficult and unsuitable for large-scale production. The hydrothermal method can also be used to prepare particles with smaller grain sizes, but it is not conducive to industrial production. The improved solid-phase method can be used to prepare lithium-ion sieves with smaller grain sizes, but it strictly limits the choice of raw materials, and the cost is high. The solid-phase method assisted by LiCl reduces the restriction on raw materials, is suitable for industrial production, and shows excellent application prospects. The template method can be used to prepare lithium-ion sieves with a larger specific surface area, which is relatively complicated but still has excellent application prospects.

Table 2. Influence of different synthesis methods on adsorption capacity.

Synthesis Methods	Sample	Li^+ Concentration (mg/L)	Adsorption Capacity (mg/g)	Equilibrium Time (h)	Ref.
Hydrothermal method	LiOH solution	2138	76.7	24	[49]
Solid-phase method	LiCl solution	282.5	30.9	192	[62]
Sol-gel method	LiOH solution	4000	27.4	22	[63]
Improved solid-phase method	West Taijinar Salt Lake brine	669	24.97	24	[65]
Solid-phase method assisted by a LiCl molten salt	LiOH solution	280	≈33	5	[66]
Template method	Li^+ solution	56	70	4	[67]

3.3. The Influence of Acid Leaching

Li^+ in Li_2TiO_3 undergoes ion exchange with H^+ ions in acid solutions to generate H_2TiO_3 . The acid solution elution process has an important influence on the adsorption performance of lithium-ion sieves. Most scholars choose HCl as the eluent, and few have explored the use of other eluents.

Wang et al. [68] modified the eluent from HCl to a weak polybasic acid and found that citric acid (CA) is an ideal eluent. As shown in Figure 9, CA can significantly reduce damage caused to the structure of H_2TiO_3 . The titanium loss is only 0.27%, the elution rate of Li^+ ions reaches 95.5%, and the lithium concentration in the elution solution is increased up to 4.06 g/L. CA can also lead to an adsorption capacity for H_2TiO_3 of up to 52 mg/g, which indicates that it is an ideal eluent.

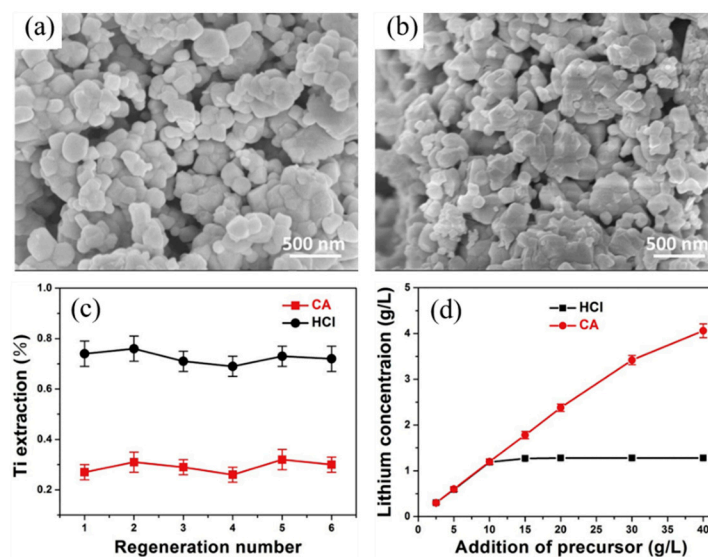


Figure 9. Schematic illustration of different acids eluting lithium-ion sieves: (a) H_2TiO_3 eluted by CA; (b) H_2TiO_3 eluted by HCl; (c) loss amount of titanium; (d) lithium concentration [68].

Ji et al. [51] chose sodium persulfate as the eluent, and the elution rate of Li^+ ions was found to be higher than that of the HCl solution. As shown in Figure 10, H_2TiO_3 presents a spherical morphology, and the adsorption capacities in pure lithium solution are 26.90 mg/g, 20.23 mg/g, and 18.50 mg/g in sequence. Coexisting cations, such as Na^+ , K^+ , and Mg^{2+} , have little effect on the adsorption performance. During the first elution process, the extraction amount of lithium is near to the theoretical value. This value is close to the platform value in the first 60 min for the hydrolysis of sodium persulfate. The amount of titanium lost is gradually decreased. Li_2TiO_3 eluted with 0.8 mol/L $\text{Na}_2\text{S}_2\text{O}_8$ showed a better application performance.

Table 3 lists the results obtained for using different acids to treat the Li_2TiO_3 precursor. Different eluents show different levels of Li^+ uptake and Ti^{4+} loss. It can be observed from the table that different acids show higher Li^+ -ion elution rates, and HCl, $\text{H}_2\text{C}_2\text{O}_4$, citric acid, and sodium persulfate all show Li^+ -ion elution rates of more than 94%. However, the Ti^{4+} dissolution loss for HCl and citric acid is relatively small, which will not lead to significant damage to the structure, and the lithium-ion sieves can be reused. The dissolution loss of Ti^{4+} for $\text{H}_2\text{C}_2\text{O}_4$ and sodium persulfate is relatively high, which will lead to greater damage to the structure. Therefore, both HCl and citric acid are ideal eluents for Li^+ ions.

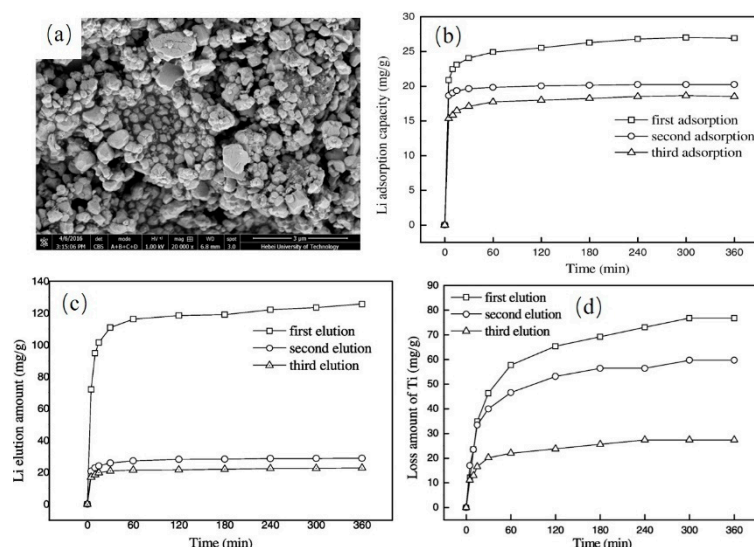


Figure 10. Li_2TiO_3 eluted by $Na_2S_2O_8$: (a) H_2TiO_3 ; (b) adsorption capacity; (c) lithium elution amount; (d) loss amount of Ti [51].

Table 3. The results obtained for using different acids to treat the Li_2TiO_3 precursor.

Eluent	Li^+ Uptake (%)	Ti^{4+} Loss (%)	Ref.
HCl	94.7	0.74	[68]
H_2BO_3	84.6	0.71	[68]
H_3PO_3	93.4	2.96	[68]
H_2SO_3	91.8	1.9	[68]
$H_2C_2O_4$	95.3	21.26	[68]
$C_4H_6O_4$	88.7	1.4	[68]
Citric acid	95.5	0.27	[68]
Sodium persulfate	98.8	≈ 17.5	[51]

3.4. Other Influences

The adsorption performance of the H_2TiO_3 adsorbent depends not only on the properties and specific surface area of the material itself but also on the adsorption environment. For example, the external environment, such as adsorption temperature and stirring, the quantity of lithium-ion sieves, the pH value of the brine, the type and amount of anions and cations, organic matter, etc. Appropriate adjustment of these influencing factors can provide an ideal adsorption environment for the adsorption process, effectively improving the adsorption performance. It can provide theoretical guidance for the adsorption environment in industrial applications and achieve the purpose of efficient adsorption.

4. Efficient Recycling

The efficient recycling of the H_2TiO_3 lithium-ion sieve is the premise for reuse. However, H_2TiO_3 with a large specific surface area is often prepared into nanoparticles, making its recycling challenging. Below, several examples of efficient recycling are reviewed based on doping, support, and other effective methods.

4.1. Doping

In response to recycling difficulties, Wang et al. [69] synthesized an effective Fe-doped lithium titanium oxide via solid-phase reactions followed by acid treatment to form an iron-doped lithium-ion sieve. The resulting solid powder displays both a superior adsorption capacity for lithium and high separation efficiency for the adsorbent from the solution. In a typical procedure, $LiOH \cdot H_2O$, TiO_2 , and Fe_2O_3 were weighed and ground according to the

stoichiometric molar ratio (Li: Ti: Fe = 2:1:0.15), and the powders were ground for 20 min in an agate mortar. The ground solids were calcined at 600 °C for 3 h, resulting in light brown to brown solid powders. The obtained Fe-doped Li_2TiO_3 was treated with 0.5 mol/L HCl solution at 30 °C for 24 h, washed, and dried to prepare the Fe-doped lithium-ion sieves. As shown in Figure 11, the particle grains show a uniform Fe distribution, the primary particles range in size from 100 to 200 nm, the mean size of the secondary agglomeration particles is 28.6 μm , and the BET surface area is 47.85 m^2/g compared to 28.17 m^2/g without Fe doping. The equilibrium adsorption capacity in the LiOH solution reaches 53.3 mg/g within 24 h, which is higher than that of pristine Li_2TiO_3 (50.5 mg/g) without Fe doping. The saturated magnetization value for Fe-doped H_2TiO_3 is 13.76 emu/g, enabling effective separation of the material from solid suspensions through the use of a magnet with a separation efficiency of 96% or better, which can be applied at a large scale and continuously removed from the LiOH solution.

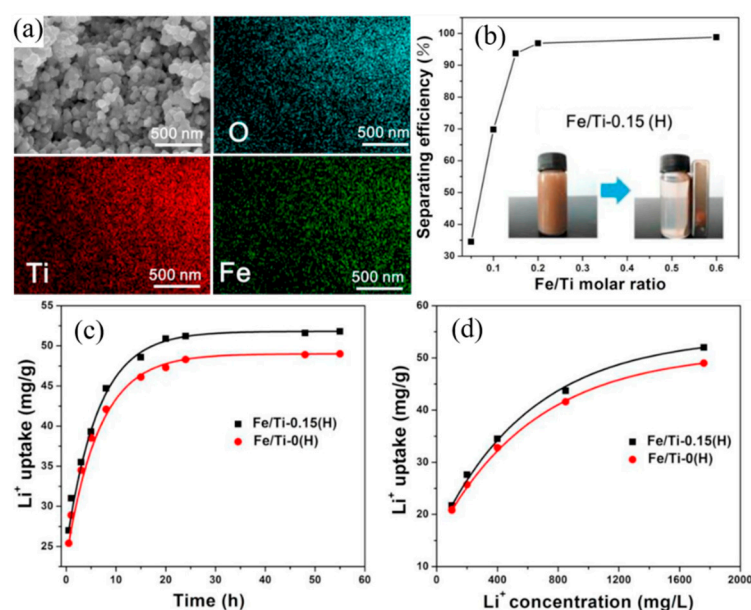


Figure 11. Iron-doped lithium-ion sieves: (a) O, Ti, and Fe elemental mapping; (b) separation efficiency for varying Fe/Ti molar ratios; (c) adsorption capacity at different times; (d) adsorption capacity for a varying Li^+ concentration [69].

4.2. Supports

Support is a commonly used method to avoid the loss of nanomaterials. Nanomaterials supported on a carrier can improve the scattering, reduce the amount of nanomaterials required, improve mechanical strength, and enable easier recycling. Typical carriers include carbon, polymers, ceramics, etc.

Yu et al. [70] prepared a peculiar shuttle-like nanosized Li_2TiO_3 lithium-ion sieve by using a hydrothermal method, uniformly mixing with $\text{C}_6\text{H}_8\text{O}_7 \cdot \text{H}_2\text{O}$ with a molar ratio of 1:1, and then calcination at 1100 °C under a N_2 atmosphere to obtain a $\text{Li}_2\text{TiO}_3/\text{C}$ block. The block $\text{H}_2\text{TiO}_3/\text{C}$ lithium-ion sieve was obtained by eluting in 0.2 mol/L HCl solution at 100 °C for 24 h. As shown in Figure 12, there are rich pores with different sizes present on the surface and interior of $\text{H}_2\text{TiO}_3/\text{C}$, and it can be inferred that the solution mobility will be enhanced. The shuttle-like nanosized H_2TiO_3 grains are evenly distributed on the porous carbon membrane surface, and the H_2TiO_3 grains are shuttle-like with completely exposed surfaces and uniform distributions with average lengths and diameters of 172 nm and 52 nm, respectively. The adsorption capacity of $\text{H}_2\text{TiO}_3/\text{C}$ can reach 80% of the equilibrium value after ~2 h of adsorption, indicating a higher adsorption efficiency. Similar adsorption behaviour is exhibited under various conditions. The $\text{H}_2\text{TiO}_3/\text{C}$ lithium-ion sieve shows good stability, recyclability, and excellent selective adsorption performance.

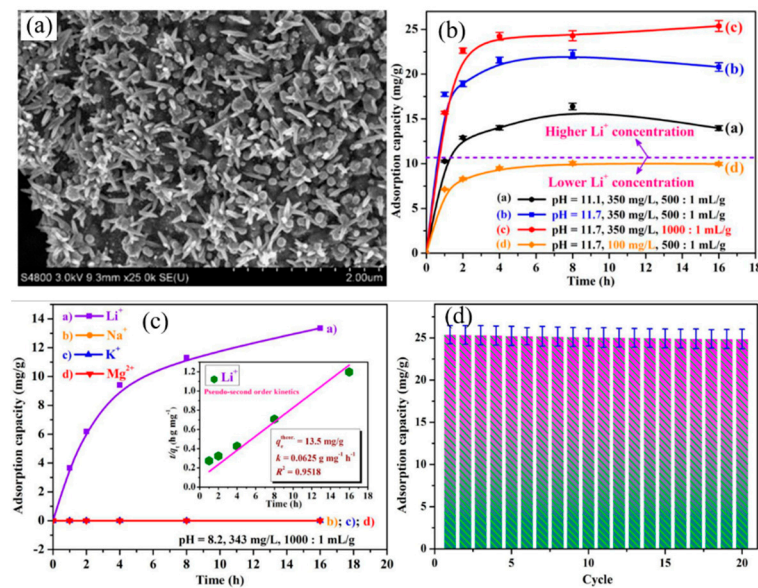


Figure 12. Peculiar shuttle-like $\text{H}_2\text{TiO}_3/\text{C}$ lithium-ion sieve: (a) porous carbon membrane loaded with shuttle-like nanosized $\text{TiO}(\text{OH})_2$ grains; (b) adsorption capacity curves for $\text{TiO}(\text{OH})_2/\text{C}$ LIS at varying pH values; (c) adsorption capacity curves for $\text{TiO}(\text{OH})_2/\text{C}$ lithium ion sieves with different cations; (d) cycling performance of $\text{TiO}(\text{OH})_2/\text{C}$ LIS [70].

Lawagon et al. [71] used polymers as supports to prepare lithium-ion sieves. He synthesized Li_2TiO_3 using solid-phase methods and then supported it onto a polymer by using electrospinning technology, as shown in Figure 13. Compared with other $\text{H}_2\text{TiO}_3/\text{polymer}$ nanofibres, $\text{H}_2\text{TiO}_3/\text{PANs}$ show the largest specific surface area of $3.9 \text{ m}^2/\text{g}$ and exhibit good hydrophilicity and the best adsorption capacity. $\text{H}_2\text{TiO}_3/\text{PANs}$ show an excellent recycling performance, which shows application potential.

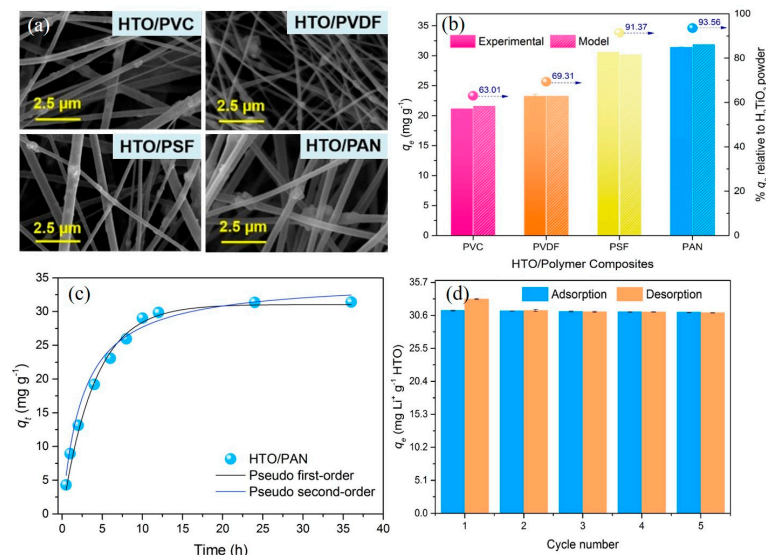


Figure 13. $\text{H}_2\text{TiO}_3/\text{polymer}$ NF lithium-ion sieve: (a) $\text{H}_2\text{TiO}_3/\text{polymer}$ nanofibre; (b) experimental and predicted adsorption capacity of different $\text{H}_2\text{TiO}_3/\text{polymer}$ composites; (c) adsorption capacity of $\text{H}_2\text{TiO}_3/\text{PAN}$ NFs; (d) cycling performance of $\text{H}_2\text{TiO}_3/\text{PAN}$ NFs [71].

Limjuco et al. [72] used soft poly(vinyl alcohol) (PVA) as a support to prepare the $\text{H}_2\text{TiO}_3/\text{PVA}$ lithium-ion sieve, as shown in Figure 14. Anatase-type TiO_2 and Li_2CO_3 (2:1 Li/Ti molar ratio) precursors were mixed, ground, and thermally treated in air using an alumina crucible to obtain Li_2TiO_3 powder. The Li_2TiO_3 powder was delithiated using

0.2 M HCl for 24 h (1 g/L) to obtain H_2TiO_3 as a lithium-ion sieve. The H_2TiO_3 powder is poured into the dissolved PVA, and the foaming agent is gradually added, accompanied by vigorous stirring. The mixture expands to twice its original volume due to effective froth formation. $\text{H}_2\text{TiO}_3/\text{PVA}$ has a porous structure, good mechanical properties and hydrophilicity, and the adsorption capacity is only slightly lower than that of H_2TiO_3 powder. Similar to a sponge, $\text{H}_2\text{TiO}_3/\text{PVA}$ can realize the in and out flow of brine by extrusion. $\text{H}_2\text{TiO}_3/\text{PVA}$ has good Li^+ -ion selectivity and recycling performance.

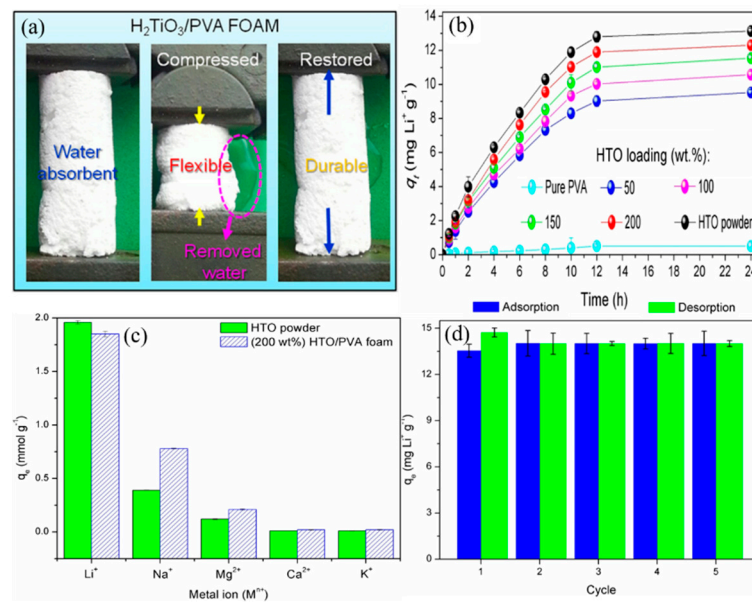


Figure 14. $\text{H}_2\text{TiO}_3/\text{PVA}$ lithium-ion sieve: (a) $\text{H}_2\text{TiO}_3/\text{PVA}$ lithium-ion sieve before, during, and after compression; (b) adsorption capacity of the lithium-ion sieve; (c) metal ion uptake of the lithium-ion sieve; (d) adsorption–desorption cycling performance [72].

Ceramic foam is also an ideal support material. Zhang et al. [73] supported H_2TiO_3 on ceramic foams using the sol-gel method, as shown in Figure 15. Kaolin, talc powder, and alumina were used as raw materials, and ceramic foams were directly prepared using a foaming agent. CH_3COOLi and $\text{Ti}(\text{OC}_4\text{H}_9)_4$ are lithium and titanium sources, respectively. After the Li_2TiO_3 sol was prepared using the sol-gel method, the ceramic foams were placed into the sol and then dried at 80 °C for 5 h to form a gel. The gel was uniformly distributed on the ceramic foams and calcined at 650 °C for 2 h. The H_2TiO_3 -lithium adsorbent was obtained after hydrochloric acid modification, filtration, washing, and drying. The adsorptive capacity was found to reach a value of up to 21.0 mg/g. The H_2TiO_3 loaded onto ceramic foams solves the problem encountered by Li_2TiO_3 powders in engineering applications.

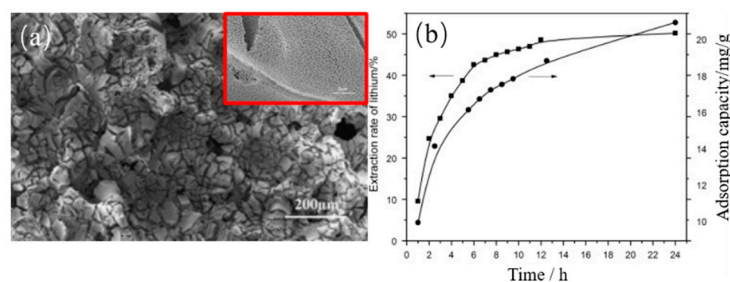


Figure 15. Li_2TiO_3 loaded onto ceramic foams: (a) Li_2TiO_3 loaded onto ceramic foams; (b) extraction rate for Li^+ and adsorption capacity of H_2TiO_3 -lithium adsorbent loaded onto ceramic foams [73].

4.3. Large Particles

Large-particle lithium-ion sieves with porous structures have a high adsorption capacity and good separation ability. Chen et al. [74] synthesized a Ti-based ion sieve (PIS) with a mesoporous structure through an agar-assisted strategy, as shown in Figure 16. The H_2TiO_3 adsorbent prepared using the solid-phase method and agar were loaded in 15 mL deionized water and then heated to 100 °C with simultaneous stirring until the agar was completely molten. The slurry was immediately dropped into cold simethicone via an injector to obtain an ion sieve (IS). Moreover, the corresponding PIS was acquired after the calcination of IS spheres at 550 °C for 1 h in air. The specific surface area of PIS was 102.78 m^2/g , which convincingly confirms the generation of a porous structure in the thermal process. The pore diameters for the PIS were found to be mainly distributed in the range of 3–5 nm, demonstrating its uniform mesoporous structure. PIS has an adsorption capacity of 25.8 mg/g in geothermal water, and the adsorption equilibrium time is approximately 6 h. The PIS successfully improves the postseparation performance of Ti-LIS with a guaranteed high capacity and fast kinetics and can be regarded as a promising candidate for lithium recovery from geothermal water and even salty seawater.

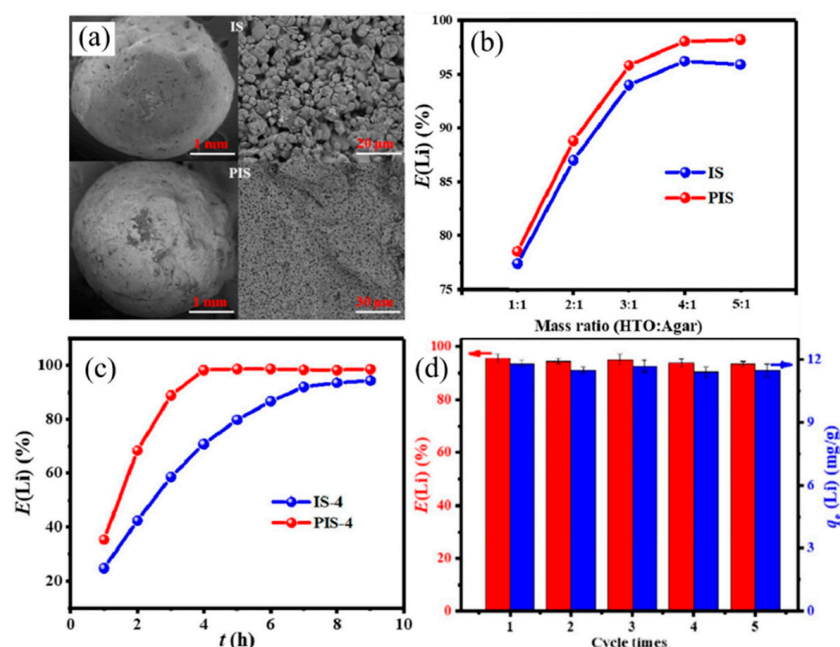


Figure 16. IS and porous PIS spheres: (a) macromorphology and micromorphology; (b) lithium adsorption efficiency for an IS and PIS with different mass ratios of lithium-ion sieve; (c) lithium adsorption efficiency at different times; (d) desorption performance and reusability of PIS-4 in geothermal water [74].

Table 4 lists a comparison of recyclable Li^+ adsorbents. Different recovery methods for lithium-ion sieves have certain advantages. It can be seen that the use of different recovery methods has no significant influence on the adsorption capacity, and the adsorption equilibrium time is relatively long, which is not practical for industrial applications. Therefore, it is necessary to develop H_2TiO_3 lithium-ion sieves, which can be recycled and adsorbed efficiently.

Table 4. Comparison of recyclable Li⁺ adsorbents.

Recycling Method	Adsorbent	Sample	Li ⁺ Concentration (mg/L)	Adsorption Capacity (mg/g)	Equilibrium Time (h)	Ref.
Doping	Fe-doped H ₂ TiO ₃	LiOH solution	1800	53.3	20	[69]
	HTO/C	Li ⁺ solution	350	22.4	16	[70]
Supported	HTO/PANs	LiOH solution	70	31–32	24	[71]
	HTO/PVA	LiCl/LiOH solution	7	12	12	[72]
	HTO/Ceramic foams	LiOH solution	2000	21	12	[73]
	PVC-HTO	Geothermal water	25.78	11.35	12	[75]
Larger particles	HTO-agar assist	Geothermal water	25.8	12.29	6	[74]

5. Conclusions and Outlook

H₂TiO₃ lithium-ion sieve is a layered double hydroxide with a 3R₁ sequence to arrange oxygen layers. Its adsorption mechanism involves the breaking of surface O-H bonds and the formation of O-Li bonds. H₂TiO₃ lithium-ion sieves prepared from anatase in a reasonable method show the largest adsorption capacity. Different recovery methods have no significant influence on the adsorption capacity. As a new type of lithium adsorbent, it has many advantages and is suitable for lithium extraction from salt lake brine. However, titanium-based lithium-ion sieves have not been applied in industry, and their research lags far behind that for other lithium-ion sieves. Many problems need to be studied in depth.

H₂TiO₃ has become the most promising lithium-ion sieve at this stage. However, many challenges remain before it can be industrialized, which are summarized as follows: (1) H₂TiO₃ is usually used in powder form, which will lead to high pressure drops and energy consumption. When the powdery material is filtered, the pressure drop is obvious, the energy consumption increases, and the filtering time is long, which is not conducive to practical production and application. So, we need to prepare large-particle lithium-ion sieves with a large specific surface area to overcome the problems encountered. (2) There is no unified standard for the adsorption process. Different scholars have determined the adsorption capacity via different adsorption processes, and adsorption processes seriously influence the adsorption capacity. This results in poor comparability for the data and makes it difficult to determine whether a particular method is suitable. Therefore, it is necessary to establish a unified standard for the adsorption process of H₂TiO₃ lithium-ion sieves to promote their development. (3) Eluent is widely used during synthesis and recycling processes, which will cause damage to the environment. Therefore, it is significant to recycle the eluent or develop an environmentally friendly eluent. (4) The separation and recycling of the H₂TiO₃ lithium-ion sieve is a vital assessment index for industrial applications. Efficient separation and recycling can effectively reduce costs and have substantial economic benefits. Lithium adsorbents with high-efficiency adsorption and recovery still need to be explored further.

Author Contributions: Y.L.: conceptualization, writing–review and editing, funding acquisition, and supervision. Z.Y.: conceptualization, writing–original draft, writing–review, and editing. P.M.: conceptualization, writing, reviewing, and editing. All authors have read and agreed to the published version of the manuscript.

Funding: The authors appreciate financial support from the National Natural Science Foundation of China (Project Nos. 51774076, 51834004, 51904068, and 51474057).

Data Availability Statement: The data presented in this study are available within the article.

Conflicts of Interest: The authors declare no conflict of interest.

References

1. Wang, Y.; He, P.; Zhou, H. Olivine LiFePO₄: Development and future. *Energ. Environ. Sci.* **2011**, *4*, 805–817. [[CrossRef](#)]
2. Li, L.; Wu, L.; Wu, F.; Song, S.; Zhang, X.; Fu, C.; Yuan, D.; Xiang, Y. Review-Recent research progress in surface modification of LiFePO₄ cathode materials. *J. Electrochem. Soc.* **2017**, *164*, A2138–A2150. [[CrossRef](#)]
3. Marincas, A.; Goga, F.; Dorneanu, S.; Ilea, P. Review on synthesis methods to obtain LiMn₂O₄-based cathode materials for Li-ion batteries. *J. Solid State Electr.* **2020**, *24*, 473–497. [[CrossRef](#)]
4. Mao, F.; Guo, W.; Ma, J. Research progress on design strategies, synthesis and performance of LiMn₂O₄-based cathodes. *RSC Adv.* **2015**, *5*, 15248–15258. [[CrossRef](#)]
5. Li, J.; Li, Y.; Guo, Y.; Lv, J.; Yi, W.; Ma, P. A facile method to enhance electrochemical performance of high-nickel cathode material Li(Ni_{0.8}Co_{0.1}Mn_{0.1})O₂ via Ti doping. *J. Mater. Sci. Mater. Electron.* **2018**, *29*, 10702–10708. [[CrossRef](#)]
6. Li, J.; Li, Y.; Ma, P. A facile method to improve electrochemical performances of nickel-rich cathode material Li(Ni_{0.6}Co_{0.2}Mn_{0.2})O₂ by blending with solid electrolyte. *Mater. Res. Express* **2019**, *6*, 66314. [[CrossRef](#)]
7. Li, J.; Li, Y.; Yi, W.; Ma, P. Improved electrochemical performance of cathode material LiNi_{0.8}Co_{0.1}Mn_{0.1}O₂ by doping magnesium via co-precipitation method. *J. Mater. Sci. Mater. Electron.* **2019**, *30*, 7490–7496. [[CrossRef](#)]
8. Zhang, N.; Li, J.; Li, H.; Liu, A.; Huang, Q.; Ma, L.; Li, Y.; Dahn, J.R. Structural, electrochemical, and thermal properties of Nickel-Rich LiNi_xMn_yCo_zO₂ materials. *Chem. Mater.* **2018**, *30*, 8852–8860. [[CrossRef](#)]
9. Zhang, N.; Zaker, N.; Li, H.; Liu, A.; Inglis, J.; Jing, L.; Li, J.; Li, Y.; Botton, G.A.; Dahn, J.R. Cobalt-Free Nickel-Rich positive electrode materials with a core-shell structure. *Chem. Mater.* **2019**, *31*, 10150–10160. [[CrossRef](#)]
10. Liu, A.; Zhang, N.; Li, H.; Inglis, J.; Wang, Y.; Yin, S.; Wu, H.; Dahn, J.R. Investigating the effects of magnesium doping in various Ni-Rich positive electrode materials for lithium ion batteries. *J. Electrochem. Soc.* **2019**, *166*, A4025–A4033. [[CrossRef](#)]
11. Zhang, N.; Li, Y. Lithium-rich layered oxides as cathode materials: Structures, capacity origin mechanisms and modifications. *Prog. Chem.* **2017**, *29*, 373–387.
12. Zhang, N.; Li, Y.; Luo, Y.; Yang, Z.; Lu, J. Impact of LiTi₂(PO₄)₃ coating on the electrochemical performance of Li_{1.2}Ni_{0.13}Mn_{0.54}Co_{0.13}O₂ using a wet chemical method. *Ionics* **2021**, *27*, 1465–1475. [[CrossRef](#)]
13. Abd El-Aty, A.; Xu, Y.; Guo, X.; Zhang, S.; Ma, Y.; Chen, D. Strengthening mechanisms, deformation behavior, and anisotropic mechanical properties of Al-Li alloys: A review. *J. Adv. Res.* **2018**, *10*, 49–67. [[CrossRef](#)]
14. Peng, X.; Liu, W.; Wu, G. Strengthening-toughening methods and mechanisms of Mg–Li alloy: A review. *Rare Met.* **2022**, *41*, 1176–1188. [[CrossRef](#)]
15. Shu, J.; Harris, K.; Munavirov, B.; Westbroek, R.; Leckner, J.; Glavatskih, S. Tribology of polypropylene and Li-complex greases with ZDDP and MoDTC additives. *Tribol. Int.* **2018**, *118*, 189–195. [[CrossRef](#)]
16. Rim, Y.H.; Kim, M.; Baek, C.G.; Yang, Y.S. Effect of Li content in ion conductivity of lithium silicate glasses. *J. Alloys Compd.* **2020**, *827*, 154253. [[CrossRef](#)]
17. Ogiwara, T.; Noda, Y.; Shoji, K.; Kimura, O. Low-temperature sintering of high-strength β-eucryptite ceramics with low thermal expansion using Li₂O-GeO₂ as a sintering additive. *J. Am. Ceram. Soc.* **2011**, *94*, 1427–1433. [[CrossRef](#)]
18. Xiao, J.; Li, H.; Cheng, J. Structure and properties of Li₂O-Al₂O₃-SiO₂ low expansion glass ceramics containing B₂O₃. *J. Wuhan Univ. Technol. Mater. Sci. Ed.* **1999**, *14*, 41–45.
19. Li, H.; Eksteen, J.; Kuang, G. Recovery of lithium from mineral resources: State-of-the-art and perspectives—A review. *Hydrometallurgy* **2019**, *189*, 105129. [[CrossRef](#)]
20. Swain, B. Recovery and recycling of lithium: A review. *Sep. Purif. Technol.* **2017**, *172*, 388–403. [[CrossRef](#)]
21. Xu, P.; Hong, J.; Qian, X.; Xu, Z.; Xia, H.; Tao, X.; Xu, Z.; Ni, Q. Materials for lithium recovery from salt lake brine. *J. Mater. Sci.* **2021**, *56*, 16–63. [[CrossRef](#)]
22. Calvo, E.J. Electrochemical methods for sustainable recovery of lithium from natural brines and battery recycling. *Curr. Opin. Electrochem.* **2019**, *15*, 102–108. [[CrossRef](#)]
23. Zhang, W.; Mou, Y.; Zhao, S.; Xie, L.; Wang, Y.; Chen, J. Adsorption materials for lithium ion from brine resources and their performances. *Prog. Chem.* **2017**, *29*, 231–240.
24. Jang, Y.; Chung, E. Lithium adsorptive properties of H₂TiO₃ adsorbent from shale gas produced water containing organic compounds. *Chemosphere* **2019**, *221*, 75–80. [[CrossRef](#)]
25. Jang, Y.; Chung, E. Influence of alkanes on lithium adsorption and desorption of a H₂TiO₃ ion sieve adsorbent in synthetic shale gas-produced water. *Ind. Eng. Chem. Res.* **2019**, *58*, 21897–21903. [[CrossRef](#)]
26. Meng, F.; Mcneice, J.; Zadeh, S.S.; Ghahreman, A. Review of lithium production and recovery from minerals, brines, and lithium-ion batteries. *Min. Proc. Ext. Met. Rev.* **2021**, *42*, 123–141. [[CrossRef](#)]
27. Xiang, W.; Liang, S.; Zhou, Z.; Qin, W.; Fei, W. Extraction of lithium from salt lake brine containing borate anion and high concentration of magnesium. *Hydrometallurgy* **2016**, *166*, 9–15. [[CrossRef](#)]
28. Zhou, Z.; Liang, S.; Qin, W.; Fei, W. Extraction equilibria of lithium with tributyl phosphate, diisobutyl ketone, acetophenone, methyl isobutyl ketone, and 2-heptanone in kerosene and FeCl₃. *Ind. Eng. Chem. Res.* **2013**, *52*, 7912–7917. [[CrossRef](#)]
29. Pranolo, Y.; Zhu, Z.; Cheng, C.Y. Separation of lithium from sodium in chloride solutions using SSX systems with LIX 54 and Cyanex 923. *Hydrometallurgy* **2015**, *154*, 33–39. [[CrossRef](#)]
30. Bansal, B.; Chen, X.D.; Hossain, M.M. Transport of lithium through a supported liquid membrane of LIX54 and TOPO in kerosene. *Chem. Eng. Process. Process Intensif.* **2005**, *44*, 1327–1336. [[CrossRef](#)]

31. Parhi, P.K. Supported liquid membrane principle and its practices: A short review. *J. Chem.* **2013**, *2013*, 618236. [[CrossRef](#)]
32. Ooi, K.; Sonoda, A.; Makita, Y.; Chitrakar, R.; Tasaki-Handa, Y.; Nakazato, T. Recovery of lithium from salt-brine eluates by direct crystallization as lithium sulfate. *Hydrometallurgy* **2017**, *174*, 123–130. [[CrossRef](#)]
33. Zavahir, S.; Elmakki, T.; Gulied, M.; Ahmad, Z.; Al-Sulaiti, L.; Shon, H.K.; Chen, Y.; Park, H.; Batchelor, B.; Han, D.S. A review on lithium recovery using electrochemical capturing systems. *Desalination* **2021**, *500*, 114883. [[CrossRef](#)]
34. Battistel, A.; Palagonia, M.S.; Brogioli, D.; La Mantia, F.; Trócoli, R. Electrochemical methods for lithium recovery: A comprehensive and critical review. *Adv. Mater.* **2020**, *32*, 1905440. [[CrossRef](#)]
35. Zhou, G.; Chen, L.; Chao, Y.; Li, X.; Luo, G.; Zhu, W. Progress in electrochemical lithium ion pumping for lithium recovery. *J. Energy Chem.* **2021**, *59*, 431–445. [[CrossRef](#)]
36. Zhong, J.; Lin, S.; Yu, J. Effects of excessive lithium deintercalation on Li⁺ adsorption performance and structural stability of lithium/aluminum layered double hydroxides. *J. Colloid Interf. Sci.* **2020**, *572*, 107–113. [[CrossRef](#)]
37. Jiang, H.; Yang, Y.; Sun, S.; Yu, J. Adsorption of lithium ions on lithium-aluminum hydroxides: Equilibrium and kinetics. *Can. J. Chem. Eng.* **2019**, *98*, 544–555. [[CrossRef](#)]
38. Hamzaoui, A.H.; Hammi, H.; Nif, A.M. Operating conditions for lithium recovery from natural brines. *Russ. J. Inorg. Chem.* **2007**, *52*, 1859–1863. [[CrossRef](#)]
39. Li, J.; Luo, Q.; Dong, M.; Nie, G.; Liu, Z.; Wu, Z. Synthesis of granulated Li/Al-LDHs adsorbent and application for recovery of Li from synthetic and real salt lake brines. *Hydrometallurgy* **2022**, *209*, 105828. [[CrossRef](#)]
40. Yang, F.; Chen, S.; Shi, C.; Xue, F.; Zhang, X.; Ju, S.; Xing, W. A facile synthesis of hexagonal spinel λ -MnO₂ ion-sieves for highly selective Li⁺ adsorption. *Processes* **2018**, *6*, 59. [[CrossRef](#)]
41. Gao, A.; Sun, Z.; Li, S.; Hou, X.; Li, H.; Wu, Q.; Xi, X. The mechanism of manganese dissolution on Li_{1.6}Mn_{1.6}O₄ ion sieves with HCl. *Dalton Trans.* **2018**, *47*, 3864–3871. [[CrossRef](#)] [[PubMed](#)]
42. Luo, G.; Zhu, L.; Li, X.; Zhou, G.; Sun, J.; Chen, L.; Chao, Y.; Jiang, L.; Zhu, W. Electrochemical lithium ions pump for lithium recovery from brine by using a surface stability Al₂O₃-ZrO₂ coated LiMn₂O₄ electrode. *J. Energy Chem.* **2022**, *69*, 244–252. [[CrossRef](#)]
43. Zhou, G.; Chen, L.; Li, X.; Luo, G.; Yu, Z.; Yin, J.; Fan, L.; Chao, Y.; Jiang, L.; Zhu, W. Construction of truncated-octahedral LiMn₂O₄ for battery-like electrochemical lithium recovery from brine. *Green Energy Environ.* **2022**, *in press*. [[CrossRef](#)]
44. Zhang, Q.; Li, S.; Sun, S.; Yin, X.; Yu, J. Lithium selective adsorption on low-dimensional titania nanoribbons. *Chem. Eng. Sci.* **2010**, *65*, 165–168. [[CrossRef](#)]
45. Wang, D.; Choi, D.; Yang, Z.; Viswanathan, V.V.; Nie, Z.; Wang, C.; Song, Y.; Zhang, J.; Liu, J. Synthesis and Li-ion insertion properties of highly crystalline mesoporous rutile TiO₂. *Chem. Mater.* **2008**, *20*, 3435–3442. [[CrossRef](#)]
46. Zhang, L.; Liu, Y.; Huang, L.; Li, N. A novel study on preparation of H₂TiO₃-lithium adsorbent with titanyl sulfate as titanium source by inorganic precipitation-peptization method. *RSC Adv.* **2018**, *8*, 1385–1391. [[CrossRef](#)]
47. Yu, C.; Wang, F.; Cao, S.; Gao, D.; Hui, H.; Guo, Y.; Wang, D. The structure of H₂TiO₃-a short discussion on “Lithium recovery from salt lake brine by H₂TiO₃”. *Dalton Trans.* **2015**, *44*, 15721–15724. [[CrossRef](#)]
48. Li, X.; Chen, L.; Chao, Y.; Chen, W.; Luo, J.; Xiong, J.; Zhu, F.; Chu, X.; Li, H.; Zhu, W. Amorphous TiO₂-derived large-capacity lithium ion sieve for lithium recovery. *Chem. Eng. Technol.* **2020**, *43*, 1784–1791. [[CrossRef](#)]
49. Wang, S.; Li, P.; Cui, W.; Zhang, H.; Wang, H.; Zheng, S.; Zhang, Y. Hydrothermal synthesis of lithium-enriched β -Li₂TiO₃ with an ion-sieve application: Excellent lithium adsorption. *RSC Adv.* **2016**, *6*, 102608–102616. [[CrossRef](#)]
50. He, G.; Zhang, L.; Zhou, D.; Zou, Y.; Wang, F. The optimal condition for H₂TiO₃-lithium adsorbent preparation and Li⁺ adsorption confirmed by an orthogonal test design. *Ionics* **2015**, *21*, 2219–2226. [[CrossRef](#)]
51. Ji, Z.; Yang, F.; Zhao, Y.; Liu, J.; Wang, N.; Yuan, J. Preparation of titanium-base lithium ionic sieve with sodium persulfate as eluent and its performance. *Chem. Eng. J.* **2017**, *328*, 768–775. [[CrossRef](#)]
52. Chitrakar, R.; Makita, Y.; Ooi, K.; Sonoda, A. Lithium recovery from salt lake brine by H₂TiO₃. *Dalton Trans.* **2014**, *43*, 8933–8939. [[CrossRef](#)]
53. Zhang, L.; Zhou, J.; He, G.; Zhou, D.; Tang, D.; Wang, F. Extraction difficulty of lithium ions from various crystal planes of lithium titanate. *J. Wuhan Univ. Technol. Mater. Sci. Ed.* **2018**, *33*, 1086–1091. [[CrossRef](#)]
54. Zhang, L.; He, G.; Zhou, D.; Zhou, J.; Yao, Q. Study on transformation mechanism of lithium titanate modified with hydrochloric acid. *Ionics* **2016**, *22*, 2007–2014. [[CrossRef](#)]
55. Liu, G.; Zhao, Z.; Ghahreman, A. Novel approaches for lithium extraction from salt-lake brines: A review. *Hydrometallurgy* **2019**, *187*, 81–100. [[CrossRef](#)]
56. Marthi, R.; Asgar, H.; Gadikota, G.; Smith, Y.R. On the structure and lithium adsorption mechanism of layered H₂TiO₃. *ACS Appl. Mater. Inter.* **2021**, *13*, 8361–8369. [[CrossRef](#)]
57. Wang, S.; Zhang, M.; Zhang, Y.; Zhang, Y.; Qiao, S.; Zheng, S. High adsorption performance of the Mo-doped titanium oxide sieve for lithium ions. *Hydrometallurgy* **2019**, *187*, 30–37. [[CrossRef](#)]
58. Marthi, R.; Smith, Y.R. Application and limitations of a H₂TiO₃-Diatomaceous earth composite synthesized from titania slag as a selective lithium adsorbent. *Sep. Purif. Technol.* **2021**, *254*, 117580. [[CrossRef](#)]
59. Zhang, L.; Zhou, D.; He, G.; Wang, F.; Zhou, J. Effect of crystal phases of titanium dioxide on adsorption performance of H₂TiO₃-lithium adsorbent. *Mater. Lett.* **2014**, *135*, 206–209. [[CrossRef](#)]

60. Li, X.; Chao, Y.; Chen, L.; Chen, W.; Luo, J.; Wang, C.; Wu, P.; Li, H.; Zhu, W. Taming wettability of lithium ion sieve via different TiO₂ precursors for effective Li recovery from aqueous lithium resources. *Chem. Eng. J.* **2020**, *392*, 123731. [[CrossRef](#)]
61. Tang, D.; Zhou, D.; Zhou, J.; Zhang, P.; Zhang, L.; Xia, Y. Preparation of H₂TiO₃-lithium adsorbent using low-grade titanium slag. *Hydrometallurgy* **2015**, *157*, 90–96. [[CrossRef](#)]
62. Shi, X.; Zhang, Z.; Zhou, D.; Zhang, L.; Chen, B.; Yu, L. Synthesis of Li⁺ adsorbent (H₂TiO₃) and its adsorption properties. *T. Nonferr. Metal. Soc.* **2013**, *23*, 253–259. [[CrossRef](#)]
63. Zhang, L.; Zhou, D.; Yao, Q.; Zhou, J. Preparation of H₂TiO₃-lithium adsorbent by the sol-gel process and its adsorption performance. *Appl. Surf. Sci.* **2016**, *368*, 82–87. [[CrossRef](#)]
64. Yu, C.; Song, J.; Ning, Q.; Jin, D.; Cheng, H. Research progress of the new H₂TiO₃ lithium ion sieve. *J. Shaanxi Univ. Sci. Technol.* **2021**, *39*, 140–152.
65. Gu, D.; Sun, W.; Han, G.; Cui, Q.; Wang, H. Lithium ion sieve synthesized via an improved solid state method and adsorption performance for West Taijinar Salt Lake brine. *Chem. Eng. J.* **2018**, *350*, 474–483. [[CrossRef](#)]
66. Zhang, Y.; Liu, J.; Yang, Y.; Lin, S.; Li, P. Preparation of granular titanium-type lithium-ion sieves and recyclability assessment for lithium recovery from brines with different pH value. *Sep. Purif. Technol.* **2021**, *267*, 118613. [[CrossRef](#)]
67. Xu, X.; Zhou, Y.; Fan, M.; Lv, Z.; Tang, Y.; Sun, Y.; Chen, Y.; Wan, P. Lithium adsorption performance of a three-dimensional porous H₂TiO₃-type lithium ion-sieve in strong alkaline Bayer liquor. *RSC Adv.* **2017**, *7*, 18883–18891. [[CrossRef](#)]
68. Wang, S.; Zhang, M.; Zhang, Y.; Zhang, Y.; Qiao, S.; Zheng, S. Application of citric acid as eluting medium for titanium type lithium ion sieve. *Hydrometallurgy* **2019**, *183*, 166–174. [[CrossRef](#)]
69. Wang, S.; Zheng, S.; Wang, Z.; Cui, W.; Zhang, H.; Yang, L.; Zhang, Y.; Li, P. Superior lithium adsorption and required magnetic separation behavior of iron-doped lithium ion-sieves. *Chem. Eng. J.* **2018**, *332*, 160–168. [[CrossRef](#)]
70. Yu, C.; Song, J.; Ning, Q.; Jin, D.; Cheng, H.; Li, H.; Liu, H.; Zhao, Z. Peculiar shuttle-like nano-sized TiO(OH)₂/C lithium ion sieve with improved adsorption rate and cycling reliability: Preparation and kinetics. *Hydrometallurgy* **2021**, *203*, 105627. [[CrossRef](#)]
71. Lawagon, C.P.; Nisola, G.M.; Cuevas, R.A.I.; Kim, H.; Lee, S.; Chung, W. Development of high capacity Li⁺ adsorbents from H₂TiO₃/polymer nanofiber composites: Systematic polymer screening, characterization and evaluation. *J. Ind. Eng. Chem.* **2019**, *70*, 124–135. [[CrossRef](#)]
72. Limjoco, L.A.; Nisola, G.M.; Lawagon, C.P.; Lee, S.; Seo, J.G.; Kim, H.; Chung, W. H₂TiO₃ composite adsorbent foam for efficient and continuous recovery of Li⁺ from liquid resources. *Colloids Surf. A Physicochem. Eng. Asp.* **2016**, *504*, 267–279. [[CrossRef](#)]
73. Zhang, L.; Zhou, D.; He, G.; Yao, Q.; Wang, F.; Zhou, J. Synthesis of H₂TiO₃-lithium adsorbent loaded on ceramic foams. *Mater. Lett.* **2015**, *145*, 351–354. [[CrossRef](#)]
74. Chen, S.; Chen, Z.; Wei, Z.; Hu, J.; Guo, Y.; Deng, T. Titanium-based ion sieve with enhanced post-separation ability for high performance lithium recovery from geothermal water. *Chem. Eng. J.* **2021**, *410*, 128320. [[CrossRef](#)]
75. Lin, H.; Yu, X.; Li, M.; Duo, J.; Guo, Y.; Deng, T. Synthesis of polyporous ion-sieve and its application for selective recovery of lithium from geothermal water. *ACS Appl. Mater. Inter.* **2019**, *11*, 26364–26372. [[CrossRef](#)]

Disclaimer/Publisher's Note: The statements, opinions and data contained in all publications are solely those of the individual author(s) and contributor(s) and not of MDPI and/or the editor(s). MDPI and/or the editor(s) disclaim responsibility for any injury to people or property resulting from any ideas, methods, instructions or products referred to in the content.